Minimax Theory and its Applications

Volume 11 (2026), No. 2s, 338 to 352

An Infrared Images-Based Hotspot Fault Detection And Mitigation Measures In Solar-Pv Using Ldpqr And Lc2rn-Agn

P. Pradeep Kumar[1], M. Rama Prasad Reddy[2]

[1]EEE Department JNTUA, Anantapuram, Andhra Pradesh, India Email: polupradeep238@gmail.com, Orcid id:0009-0008-9864-5822

[2]EEE Department, G. Pullaiah CET, Kurnool, Andhra Pradesh, India Email: mrpreddy77@gmail.com, Orcid id:0000-0002-6843-9226

Abstract

Universally,a solar photovoltaic (PV) system stands out as a leading option among the diverse range of renewable energy sources (RES). However, none of the traditional methods focused on identifying the misalignment in the Mounting Structure (MS) in the Solar Photo-Voltaic (Solar-PV). Thus, an MS alignment with hotspot detection and Mitigation Measures (MM) in solar-PV systems using Linear Dixon-Price Quadratic Regulator (LDPQR), and Log Contrastive Regularization Recurrent Neural Adaptive Gumbel Network (LC2RN-AGN) is proposed in this paper. Primarily, to optimize the PV system layout, the proposed Two-Dimensional-Exponential Gaussian Red Panda Optimization (2D-EGRPO) is used. Likewise, by using the double-bypass diodes, the Junction Box (JB) is configured. Next, the infrared images are acquired and further inputted into the pre-trained hotspot fault detection model. Initially, the noise elimination and super-resolution are done. Next, the features and temperature features are extracted and further fed into the proposed LC2RN-AGN, where the HF is obtained. Then, based on the proposed Cubic Bray-Curtis-based Penalty Quartic K-Means (CBC-PQKM), the hotspot location is identified. Then, to mitigate the hotspot effect, the heat sink is activated. Then, the mounting misalignment verification is done, followed by LDPQR-based compensation. Thus, the proposed method attained higher reliability with a peak time of 1.77s.

Keywords: Solar Photo-Voltaic (Solar-PV), Mounting Structure (MS), Hotspot Fault (HF), Renewable Energy Sources (RES), Linear Dixon-Price Quadratic Regulator (LDPQR), Log Contrastive Regularization Recurrent Neural Adaptive Gumbel Network (LC2RN-AGN) and Mitigation Measures (MM).

1. Introduction

The deployment of solar-PV systems has rapidly grown among various forms of RES owing to the low maintenance cost (Pathak et al., 2022) (Kirubakaran et al., 2022). But, through malfunctions, environmental factors affect the efficiency of the PV module (Pruthviraj et al., 2023). The hotspot effect is produced by the damage in the PV farm (Afifah et al., 2020). Thus, for upgrading the reliability of the PV systems, timely detection of PV faults is crucial. Basically, for PV system inspection and hotspot identification, Infrared Thermal Imaging (ITI) has emerged as an innovative solution (Baltacı et al., 2024) (Wang et al., 2023).

To perform hotspot classification in PV arrays, Deep Learning (DL) approaches like Convolutional Neural Network (CNN) and Recurrent Neural Network (RNN) were established (Cipriani et al., 2020) (Huerta Herraiz et al., 2020). Presently, the efficient hotspot mitigation circuit is used to diminish cell temperature under mismatch conditions via a bypass scheme (Dhimish et al., 2024). Also, to mitigate the hotspot effect, the metal-oxide-semiconductor field-effect transistors are employed (Goudelis et al., 2022).Nonetheless, none of the traditional works focused on compensating for the MS misalignment. Thus, an MSalignment with hotspot detection and MM in solar-PV systems using LDPQR and LC2RN-AGN is proposed in this paper.

1.1 Problem statement

The prevailing works' drawbacks are listed further,

- None of the traditional approaches concentrated on mitigating the MS misalignment.
- The existing (Ukiwe et al., 2024) failed to localize the hotspot region in the solar PV.

- ❖ The traditional (Amiri et al., 2024) had high energy loss and poor PV performance due to the single diode model-based JB.
- ❖ The conventional (Su et al., 2021) failed to provide MM to the corresponding HF.
- ❖ Some of the existing works had limited accuracy due to the thermal noises.

1.2 Objectives

The contributions of the proposed approach are presented below,

- ❖ The proposed LDPQR is established to compensate for the MS misalignment.
- ❖ A novel CBC-PQKM is incorporated to identify the region of the HF.
- ❖ The proposed work utilizes the double bypass diode model during JB configuration.
- ❖ An effective heat sink activation and PV system layout optimization are introduced as an MM to the HF.
- ❖ The proposed LNEDKF is used to eliminate the thermal noises from the input images.

The remaining part is structured as, in Section 2, related works are surveyed; in Section 3, the proposed mechanism is exhibited; in Section 4, the proposed method's findings is discussed; Section 5 concludes the paper.

2. Literature Survey

(Karimi et al., 2020) recommended a hotspot detection model for PV strings using a current-based approach. Here, to find the HF in PV modules, the hotspot detection index regarding the cumulative rate slope calculation was used. This approach had better efficiency, but it had biased results due to the inadequate measures.

(Xiaoni et al., 2024) applied a hotspot fault diagnosis framework for PV clusters. Here, to identify the hotspot faults, waveform characteristics of time series data were utilized. Then, to estimate the severity of the hotspot significantly, the fuzzy inference system was established. However, it had complexity and erroneous outcomes.

(Ukiwe et al., 2024) established a DL model-based hotspot classification employing electrical installations' infrared thermographic images. Here, to classify the HF in PV modules, a transfer learning-based Visual Geometry Group-16 (VGG-16) was established. This approach had high reliability but failed to localize the hotspot region.

(Amiri et al., 2024) presented the fault detection of a PV system using hybrid-DL techniques. To identify the PV faults efficiently, the CNN and Bidirectional Gated Recurrent Unit (Bi-GRU) were employed. But, owing to the single-diode model-integrated JB, it had high energy loss.

(Su et al., 2021) applied an HF detection model for PV farms. Here, to diagnose the HF in the PV system, a residual channel-wise attention gate network was utilized. This framework had high efficiency in HF detection. But, this approach failed to provide MM to the HF.

3. Proposed Methodology For Hotspot Detection And Mitigation Measures In Solar-Pv Systems

Here, by using LDPQR and LC2RN-AGN, an MSalignment with hotspot detection and MM in a solar-PV system is implemented. In Figure 1, the proposed work's pictorial depiction is given.

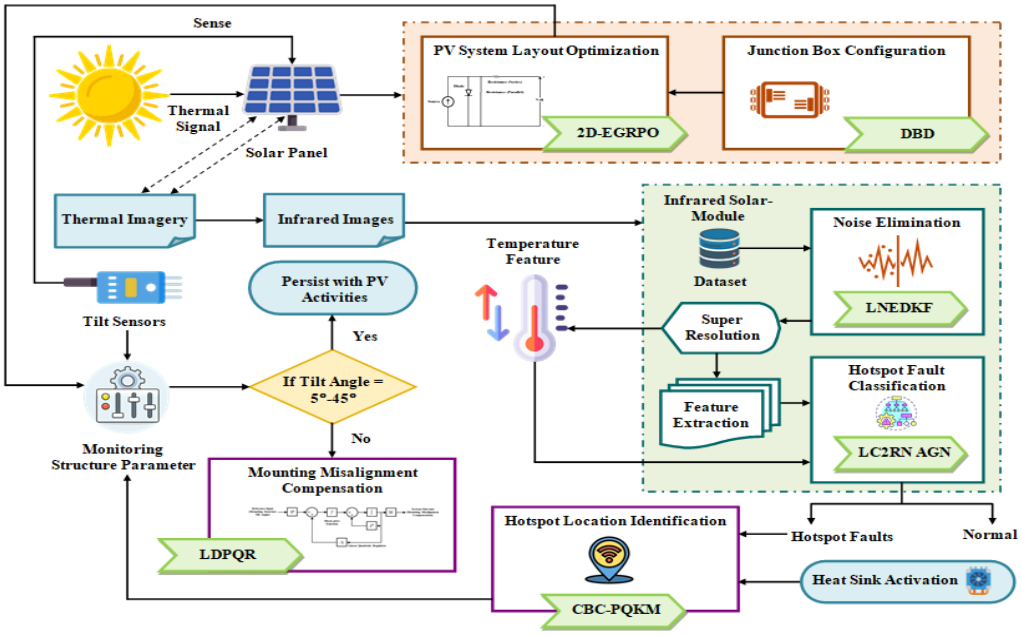


Figure 1: The structural illustration of the research methodology

3.1 Solar panel

A device composed of photovoltaic cells that convert sunlight into electricity is termed the solar panel.

3.2 PV system layout optimization

Initially, by using the Two-Dimensional-Exponential Gaussian Red Panda Optimization (2D-EGRPO), the PV system layout is designed optimally. The Red Panda Optimization (RPO) provides a precise solution to the complex issue. But, due to the random exploration, it had pre-mature convergence. Thus, in the proposed work, the 2D exponential Gaussian function is incorporated. Here, the input parameters $\left(\zeta_{p,q}\right)$like geographical location, PV module specification, and MS parameters are considered as red panda (member). Primarily, in the search space, the members are initialized.

$$\zeta_{p,q} = lw_q + \partial_{p,q} * \left(up_q + lw_q\right),\ p,q = 1 to P,Q \tag{1}$$

Here, P and Q signify the number of inputs and decision variables, respectively, $\partial_{p,q}$ proves the random value, and lw_q and up_q indicate the lower bound and upper bound, respectively. Here, the optimal candidate solution $\left(\left(\xi_{p,q}\right)^{opt}\right)$is identified by considering the fitness value $\left(\tau\infty\right)$as maximum energy yield, maximum land use efficiency, and minimum shading loss. The member's position is updated in the exploration phase based on the red panda's foraging behaviour in the wild. To optimize the convergence rate, the proposed work introduces the 2D exponential Gaussian function $\left(\wp^{\circ}\right)$.

$$\wp^{\circ}\left(\xi_{p,q},\left(\xi_{p,q}\right)^{opt}\right) = \exp\left(-\left(\xi_{p,q}{}^{2} + \left(\xi_{p,q}\right)^{opt^2}\right)\right) \tag{2}$$

$$\xi_{p,q}{}^{\Theta} = \xi_{p,q} + \wp^{\circ} * \left(\left(\xi_{p,q}\right)^{opt} - Kf \cdot \xi_{p,q}\right) \tag{3}$$

$$\xi_{p,q} = \begin{cases} \xi_{p,q}{}^{\Theta}, & IF\left(\tau\infty^{\Theta} < \tau\infty\right) \\ \xi_{p,q}, & ELSE \end{cases} \tag{4}$$

Where, Kf portrays the random number selected from the set {1, 2}, and ${\xi_{p,q}}^{\Theta}$ and ${\tau\infty}^{\Theta}$ display the new member's position and fitness value, respectively. Likewise, in the exploitation phase, the member's position is updated by mimicking the tree-climbing behavior of the red panda.

$$ {\xi_{p,q}}^{\Omega} = \xi_{p,q} + \frac{lw_q + \partial_{p,q} * \left(up_q + lw_q\right)}{itr} \tag{5} $$

$$ \xi_{p,q} = \begin{cases} {\xi_{p,q}}^{\Omega}, & IF\left(\tau\infty^{\Omega} < \tau\infty\right) \\ \xi_{p,q}, & ELSE \end{cases} \tag{6} $$

Here, itr specifies the iteration counter, and ${\xi_{p,q}}^{\Omega}$ and ${\tau\infty}^{\Omega}$ signify the updated member's position and fitness value, respectively. Therefore, the optimally designed PV layout is signified as $\left(\mathrm{O}_{PV}\right)$. The pseudocode of the proposed 2D-EGRPO is presented below,

---

Input: PV input parameters $\left(\zeta_{p,q}\right)$

Output: Optimal PV layout $\left(\mathrm{O}_{PV}\right)$

Begin

Initialize $\partial_{p,q}, lw_q, up_q, itr$ and maximum iteration itr_{mx}

Set $\left(itr = 1\right)$

While $\left(itr \le itr_{mx}\right)$

For 1 to each $\zeta_{p,q}$ do,

Initialize $\zeta_{p,q} = lw_q + \partial_{p,q} * \left(up_q + lw_q\right),\ p,q = 1 to P,Q$

Calculate fitness function $\left(\tau\infty\right)$

#exploration

Estimate $\wp^{\circ}\left(\xi_{p,q}, \left(\xi_{p,q}\right)^{opt}\right) = \exp\left(-\left({\xi_{p,q}}^{2} + \left(\xi_{p,q}\right)^{opt^2}\right)\right)$

IF $\left(\tau\infty^{\Theta} < \tau\infty\right)$

{

$${\xi_{p,q}}^{\Theta} = \xi_{p,q} + \wp^{\circ} * \left(\left(\xi_{p,q}\right)^{opt} - Kf \cdot \xi_{p,q}\right)$$

}

Else

{

$$\xi_{p,q}$$

}

End IF

#exploitation

Update position,

IF $\left(\tau\infty^{\Omega} < \tau\infty\right)$

{

$${\xi_{p,q}}^{\Omega} = \xi_{p,q} + \frac{lw_q + \partial_{p,q} * \left(up_q + lw_q\right)}{itr}$$

}

Else

{

$$\xi_{p,q}$$

}

End IF

End For

EndWhile

Return O_{PV}

End

In Figure 2, the PV cell's equivalent circuit is given.

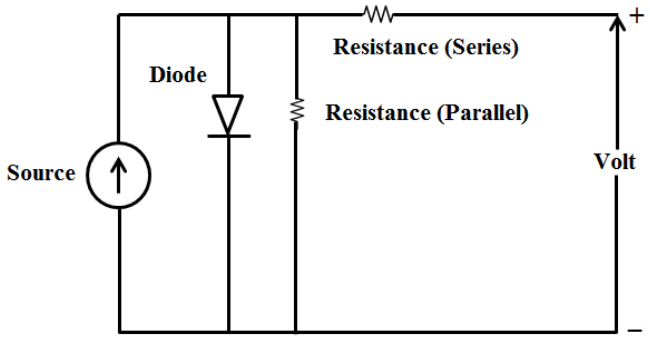


Figure 2: The circuit design of the PV cell

Furthermore, the JB configuration is explained further.

3.3 Junction box configuration

Likewise, to configure the JB to mitigate the energy loss, the Double Bypass Diode (DBD) model is utilized. The DBD has additional bypass diodes that find an alternative path to produce electricity during malfunctions.

3.4 Infrared images

Once the PV setup is designed, the infrared images (I°) are acquired from the thermography camera and then fed into the HF classification framework.

3.5 Hotspot fault classification model

Here, to diagnose the HF in the solar farms, the pre-trained HF classification framework is used.

3.5.1 Infrared solar-module dataset

Principally, to train the proposed HF detection framework, the infrared solar module dataset $(\psi_{\oplus})$ is collected.

3.5.2 Noise elimination

Next, by using the LeCun Normal with Exponential Decay Kalman Filter (LNEDKF), the thermal noises in $\psi_{\oplus}$ are eliminated. The Kalman Filter (KF) efficiently eradicates the noises in the image by analyzing the optimal state instances. But, due to the poor initialization, it had a slow convergence rate. Henceforth, the LeCun normal with exponential decay initialization (λ) is established as,

$$\lambda = \psi_{\oplus}\left(0, \frac{1}{\sqrt{\psi_{\oplus} \bullet \exp^{-ck\varpi}}}\right) \tag{7}$$

$$\kappa\eta(x,y) = \sum(j,k) \in D \sum \sigma_{j,k} \lambda(\psi_{\oplus})(x-j)(y-k) + \upsilon(x,y) \tag{8}$$

Here, $\kappa\eta$ portrays the Kalman filter, (x, y) states the image pixels, (j, k) shows the image coordinates, D shows the range of pixels, σ and υ exemplify the Kalman parameters, ck signifies the decay coefficient, and ϖ designates the layer index. Therefore, the noise-eliminated images are shown as (Fil).

3.5.3 Super-resolution

Then, the Fil is subjected to a super-resolution phase, where the low-resolution pixels of the Fil is enhanced into high-resolution pixels. The contrast-enhanced image is mentioned as (Sun).

3.5.4 Features and temperature features extraction

Then, from the Sun, features like entropy, texture, skewness, and kurtosis and temperature features like maximum temperature, temperature disparity, temperature distribution, and thermal gradient are extracted. Thus, the extracted features are illustrated as (h_g).

3.5.5 Hotspot fault classification

Then, the h_g is fed into the proposed LC2RN-AGN classifier, which predicts the HF in the PV farms. The Recurrent Neural Network (RNN) efficiently holds the past information of the sequential data. But, it had overfitting problems and vanishing gradient issues. Thus, the log contrastive regularization and adaptive Gumbel activation are incorporated into the proposed approach. In Figure 3, the LC2RN-AGN's schematic diagram is given.

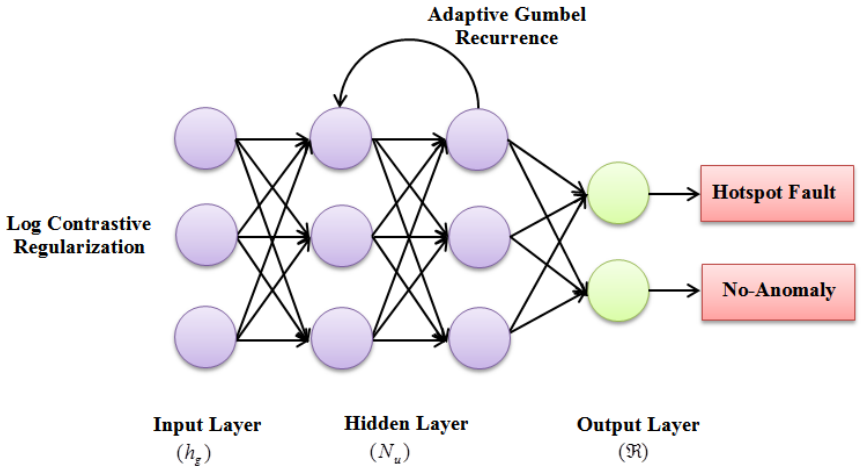


Figure 3: LC2RN-AGN's architecture

Chiefly, the input layer grasps the h_g, and then the h_g is formatted to fit into the neural network. To mitigate the vanishing gradient issue, the proposed scheme establishes the adaptive Gumbel activation $(\alpha\partial)$.

$$\alpha\partial(h_g) = 1 - \left(1 + h_g \cdot \exp(h_g)\right)^{-\frac{1}{h_g}} \tag{9}$$

Also, the hidden layers (N_u) are used to process h_g by sharing their weight (Ξ) and bias (Φ). Similarly, the recurrence operation helps to hold the past information efficiently.

$$N_u = \alpha\partial \cdot (h_g * \Xi) + \Phi \tag{10}$$

Lastly, the output layer $(\Re)$ classifies the HF as cell $(C1)$, cell-multi (Cm), hot-spot $(H1)$, hot-spot-multi (Hm), and no-anomaly (Na).

$$\Re \to \langle C1, Cm, H1, Hm, Na \rangle \quad (11)$$

The pseudo-code of the proposed LC2RN-AGN is given below,

Input: Extracted features h_g

Output: Classified HF $\Re$

Begin

Initialize $\alpha\partial$, h_g, Ξ and Φ

Perform input layer

Activate adaptive gumbel,

$$\alpha\partial(h_g) = 1 - (1 + h_g \cdot \exp(h_g))^{-\frac{1}{h_g}}$$

Execute hidden layers

$$N_u = \alpha\partial \cdot (h_g * \Xi) + \Phi$$

Evaluate output layer

IF (actual == target)

{

Stop

}

Else

{

Back propagation

}

End IF

Return $\Re \to \langle C1, Cm, H1, Hm, Na \rangle$

End

The proposed LC2RN-AGN significantly diagnoses the HF.

3.6 Hotspot location identification

Then, by using the Cubic Bray-Curtis-based Penalty Quartic K-Means (CBC-PQKM), the region of the hotspots, such as $C1, Cm, H1$, and Hm is identified. Here, according to the pixel intensities, the hotspot's region is spotted. The K-means have high computational power. But, it has time complexity and a suboptimal solution. Thus, in the proposed work, cubic-bray-curtis distance and penalty quartic function are incorporated. Initially, the $t = 1 to T$ number of data points (D_t) participated in the clustering process is initialized as,

$$D_t = |D_1, D_2, \ldots\ldots D_T| \quad (12)$$

Later, by using the penalty quartic function $(\wp q)$, the centroid (Cd) is selected among D_t, thus increasing the clustering quality.

$$\wp q(D_t) = \sum_{t=1}^{T} D_t^{\,6} - 16 D_t^{\,2} + 5 D_t + \Delta_f(D_t) \to Cd \quad (13)$$

Here, Δ_f specifies the penalty factor. Then, by using the cubic-bray-curtis distance (Bc_{dis}), the distance between the D_t and Cd is estimated.

$$Bc_{dis}\left(D_t, Cd\right) = \frac{\sum_{t=1}^{T}\left|D_t - Cd\right|^3}{\sum_{t=1}^{T}\left|D_t + Cd\right|^3} \tag{14}$$

D_t is grouped into the cluster based on the nearest distance. Lastly, the hotspot's region-identified data is mentioned as $\left(\varsigma\omega\right)$.

3.7 Heat sink activation

A heat sink is activated in the $\varsigma\omega$ to mitigate the hotspot effect. Essentially, a heat sink in solar PV is a passive device that absorbs and dissolves excess heat from PV cells, preventing overheating. Usually, the heat sink is attached to the backside of the PV panel or integrated into its internal structure. The heat sink spreads the heat across its surface and then discharges it into the surrounding environment via convection or radiation. Also, by cooling the PV panel, the heat sink maintains optimal operating temperatures, preserving the lifespan of the PV system. Therefore, the mathematical representation of the heat sink-based heat transfer is given below,

$$H_{\nabla\infty} = \left(\lambda_{con} + \chi_{rad}\right)\cdot\left(\partial^{\circ} + \mathrm{I}\lambda\cdot \mathrm{K}_f \cdot L_t\right)\left(Tem - Tem_{am}\right) \tag{15}$$

Here, $H_{\nabla\infty}$ signifies the heat sink operation, λ_{con} specifies the convective heat transfer coefficient, χ_{rad} displays the radiative heat transfer coefficient, ∂° means the base area, $\mathrm{I}\lambda$ portrays the number of fins on the heat sink, K_f displays the fin efficiency, L_t illustrates the cross-sectional area, Tem signifies the temperature of the base of the heat sink, and Tem_{am} designates the ambient temperature.

3.8 Mounting structure misalignment identification

Similarly, to analyze the impact of the hotspot in the MS, the MS misalignment identification $\left(Id\right)$ is done. Here, the MS parameter named tilt angle $\left(\mathrm{T}\alpha\right)$ is sensed via the tilt sensor.

$$Id = \begin{cases} IF\left(\mathrm{T}\alpha == 5^{\circ} to\, 45^{\circ}\right), & Normal \\ Else, & Deviation \end{cases} \tag{16}$$

If the $\mathrm{T}\alpha$ is equal to 5 to 45 degrees, then the MS is normal. Else, it is considered that the MS is misaligned $\left(\mathrm{A}_{\notin}\right)$. The common PV activities are continued whether the MS is normal. If the MS is displaced, then the MS is compensated.

3.9 Mounting misalignment compensation

Then, by using the proposed LDPQR, the MS misalignment $\mathrm{A}_{\notin}$ is compensated to improve the overall PV performance. The Linear Quadratic Regulator (LQR) had high stability and robustness. But, it struggled to select the appropriate weight values. Then, to optimize the weight values, the Dixon-Price function is utilized. In Figure 4, the LDPQR architecture is presented.

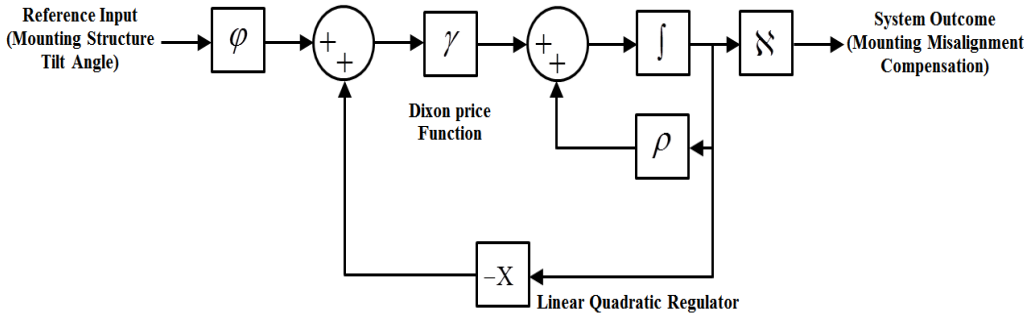


Figure 4: The LDPQR controller system

Primarily, the state vector (misaligned MS's tilt angle) and output vector (compensated MS) are assumed as below,

$$S(v) = \rho S(v) + \gamma T\alpha^{"}(v) \tag{17}$$

$$C\partial(v) = \aleph S(v) + XT\alpha^{"}(v) \tag{18}$$

Where, S means the state vector, v represents the time stamp, $C\partial$ specifies the output vector, $T\alpha^{"}$ exemplifies the input vector, and $(\rho, \gamma, \aleph, X)$ signifies the state matrices. Later, using the Dixon-price function (Dx_{pri}), the weight matrices (H_1, H_2) are selected.

$$Dx_{pri}(H_1, H_2) = (H_1 + 2)^2 + \sum_{w=1}^{W}\left((H_w - (w+1)H_{w-1})^2 + (w+1)(H_{w-1} - 1)^2\right) \tag{19}$$

Then, to minimize the cost function (performance index) $(\mu\varepsilon)$, the (H_1, H_2) is designed.

$$\mu\varepsilon = \frac{1}{2}\int_0^{\infty}\left[S^T(v)H_1S(v) + T\alpha^{"T}(v)H_2T\alpha^{"}(v)\right]d^{'}v \tag{20}$$

Here, $d^{'}$ designates the derivative parameter. Here, the feedback gain matrix (X) is computed as,

$$X = -H_2^{-1}\gamma^T Ld \tag{21}$$

Where, Ld signifies the constant coefficient. Then, to handle the system during maximum steady-state error, the pre-compensation factor (φ) is used.

$$\varphi = -\left(\aleph(\rho - \gamma X)^{-1}\gamma\right)^{-1} \tag{22}$$

Finally, the tile angle of the misaligned MS is compensated effectively, thus increasing the overall energy yield in the PV farms.

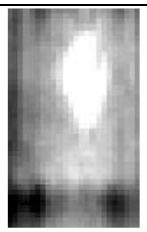
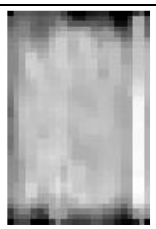
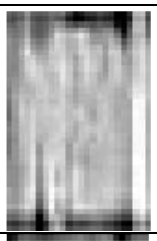
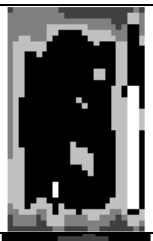
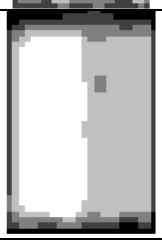
4. Results And Discussion

The performance analysis is carried out in this section to showcase the framework's dominance. To implement the proposed mechanism, the MATLAB / Simulink is used.

4.1 Dataset description

By using the Infrared Solar Modules (ISM) dataset, which contains real-world imagery of various faults found in solar arrays, the proposed work is assessed. From the whole data, 80% and 20% of data are allocated for training and testing, respectively. In Table 1, the image results of the proposed work are given.

Table 1: Image results

Class / Process	**Input**	**Noise elimination**	**Super-resolution**	**Hotspot region identification**
No-anomaly				-
Cell				
Cell-multi				
Hot-Spot				
Hot-Spot-Multi				

The image results of the proposed work regarding input, noise elimination, super-resolution, and hotspot region identification are depicted in Table 3.

4.2 Performance assessment

The performance validation of the proposed work along with existing methods is presented further.

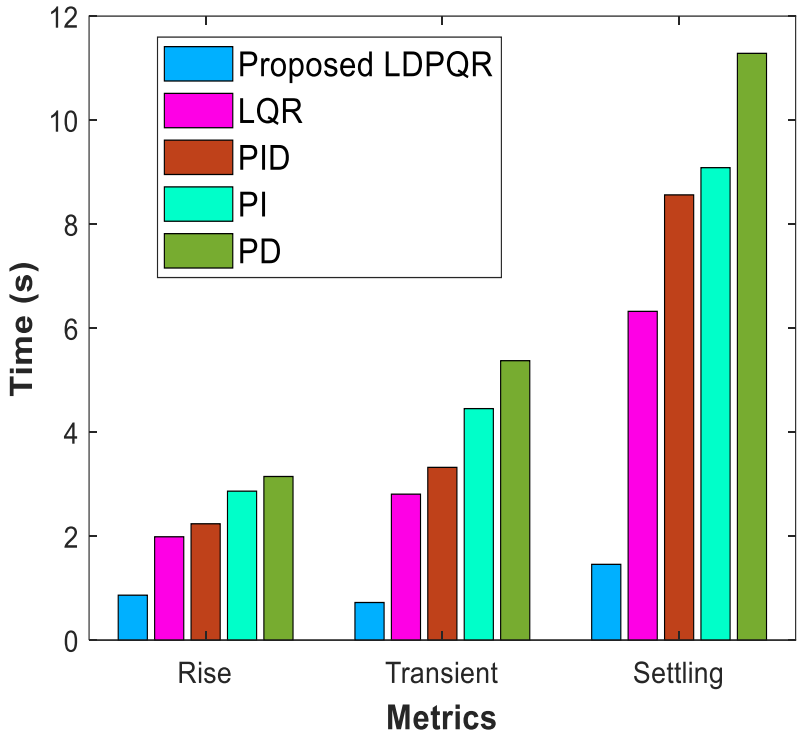


Figure 5: Performance analysis for MS misalignment compensation

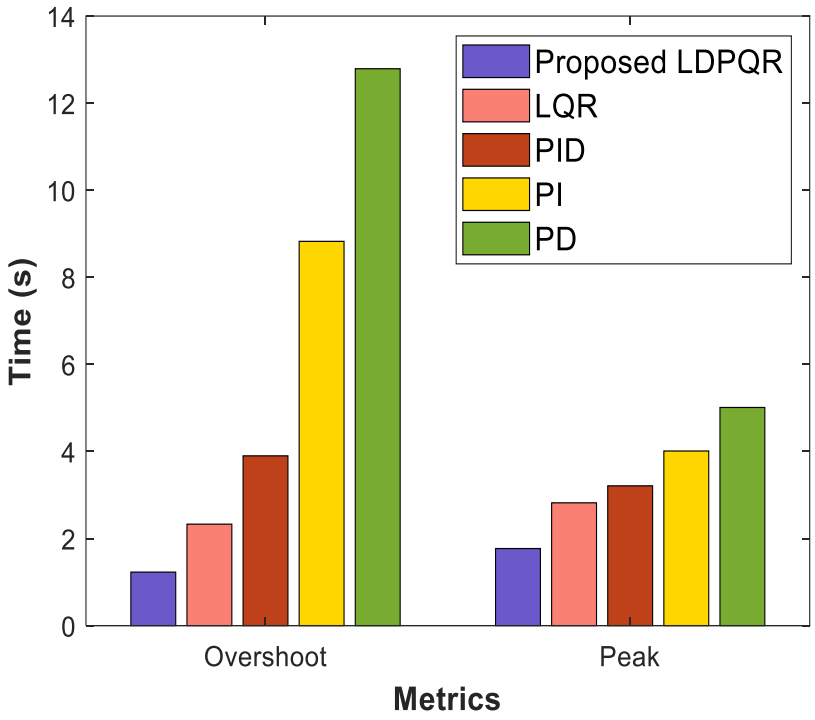


Figure 6: Performance assessment of the proposed LDPQR

The proposed LDPQR's performance is weighed against the prevailing LQR, Proportional Integral Derivative (PID), Proportional Integral (PI), and Proportional Derivative (PD) in Figures 5 and 6. Regarding rise time, transient time, settling time, overshoot, and peak time, the LDPQR achieved 0.86s, 0.72s, 1.45s, 1.22s, and 1.77s. But, the existing LQR had a 1.98s rise time and 2.82s peak time. Thus, the proposed work effectively compensates the MS misalignment.

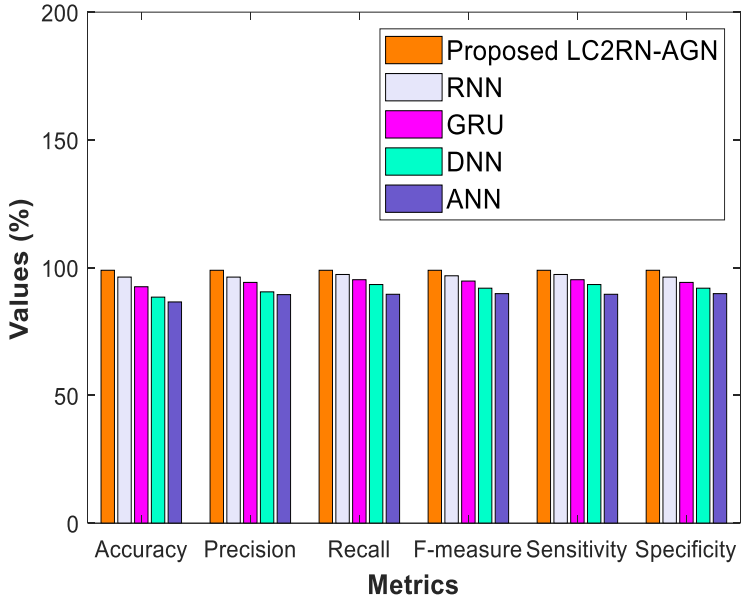


Figure 7: Performance analysis of the proposed LC2RN-AGN

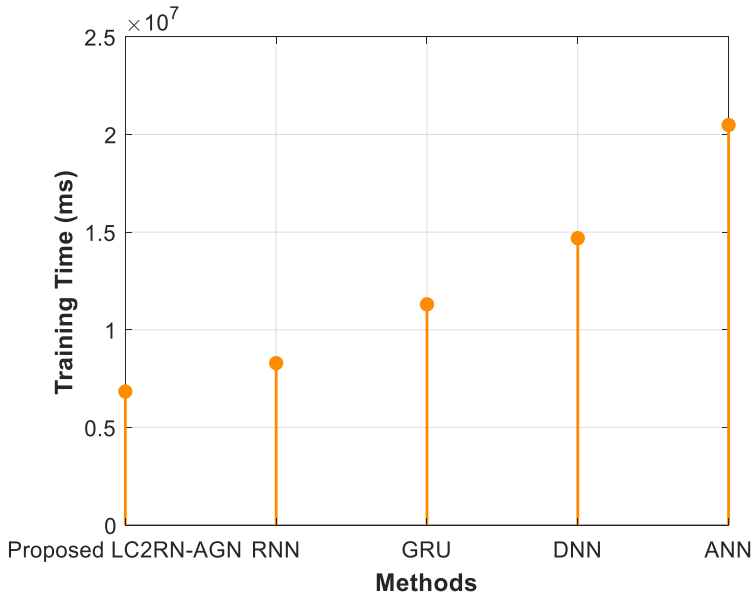


Figure 8: Training time

The adaptive gumbel activation is utilized in the proposed model to improve the classifier's efficacy. In Figures 7 and 8, the proposed LC2RN-AGN's performance is assessed by comparing it with traditional classifiers like RNN, GRU, DNN, and Artificial Neural Network (ANN). For accuracy, precision, recall, f-measure, sensitivity, specificity, and training time, the LC2RN-AGN acquired 98.9874%, 98.9842%, 98.9848%, 98.9845%, 98.9848%, 98.9842%, and 6839302ms, respectively. But, due to the overfitting issues, the conventional algorithms had lower performance. Henceforth, in HF classification, the proposed work has low time complexity and high efficiency.

Table 2: Silhouette score

Technique	**Silhouette score**
Proposed CBC-PQKM	0.984
K-means	0.942
K-medoid	0.902
FCM	0.873

SC	0.842

Table 3: Clustering time

Technique	Clustering time (ms)
Proposed CBC-PQKM	5429
K-means	7840
K-medoid	8462
FCM	10934
SC	11342

the comparative assessment of the proposed CBC-PQKM and conventional methods like K-means, K-medoid, Fuzzy-C-Means (FCM), and Spectral Clustering (SC) regarding silhouette score and clustering time are exhibited in Tables 2 and 3. For silhouette score and clustering time, the CBC-PQKM has a 0.984 and 5429ms; while, the prevailing SC achieved 0.842 and 11342ms, respectively. Thus, in HF location identification, the proposed approach has impressive results.

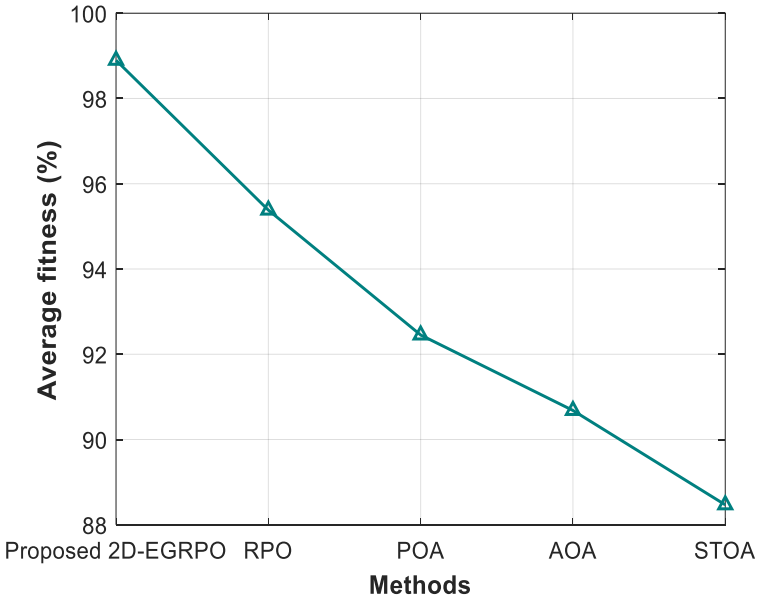


Figure 9: Average fitness

In Figure 9, the average fitness of the proposed 2D-EGRPO and conventional techniques like RPO, Pufferfish Optimization Algorithm (POA), Addax Optimization Algorithm (AOA), and Siberian Tiger Optimization Algorithm (STOA) is analyzed. The proposed 2D-EGRPO had an average fitness of 98.897%, whereas the existing STOA had an average fitness of 88.468%. Collectively, the proposed method has superior outcomes.

4.3 Comparative evaluation

The comparative analysis of the proposed work is given below,

Table 4: Comparative evaluation

Authors' name	Method	Accuracy (%)	F-measure (%)
Proposed work	LC2RN-AGN	98.987	98.984
(Sridharan & Sugumaran, 2021)	CNN	94.60	-
(Su et al., 2022)	Bidirectional Attention Feature Pyramid Network (BAFPN) and faster-region-CNN	-	98.70
(Ali et al., 2020)	Support Vector Machine	96.8	97.75

	(SVM)		
(Wu & Hao, 2023)	Selective Kernel-Faster RCNN	79.98	-
(Winston et al., 2021)	Feed forward back propagation neural network and SVM	93	-

In Table 4, the comparative assessment of the proposed framework and associated works is given. In HF classification, the proposed LC2RN-AGN had 98.987% accuracy and 98.984% f-measure. Similarly, the existing (Ali et al., 2020) utilized the SVM, which classified the PV faults with 96.8% accuracy and 97.75% f-measure. But, due to the overfitting issues, the existing works had limited performance. Thus, the proposed framework had better prominence.

5. CONCLUSION

Here, an MS-aligned LDPQR and LC2RN-AGN-centric hotspot detection and MM in the solar-PV system is proposed employing infrared images. The proposed LDPQR proficiently compensated for the MS misalignment, improving the PV's reliability. Also, to identify the HF, the LC2RN-AGN was established, thus resulting in adequate maintenance planning. Besides, the proposed work had a 1.77s peak time and 98.987% accuracy, showing better efficacy and significance. The proposed methods significantly diagnosed the HF and provided effective MM. However, this method only focused on HF in solar-PV via infrared images.

Future scope

Other types of PV faults like open-circuit, arc-fault, and short-circuit will be diagnosed using multi-modality images in the future.

REFERENCES

1. **Dataset:**https://www.kaggle.com/datasets/marcosgabriel/infrared-solar-modules

2. Afifah, A. N. N., Indrabayu, Suyuti, A., &Syafaruddin. (2020). Hotspot Detection in Photovoltaic Module using Otsu Thresholding Method. *2020 IEEE International Conference on Communication, Networks and Satellite, Comnetsat 2020 - Proceedings*, 408–412. https://doi.org/10.1109/Comnetsat50391.2020.9328987

3. Ali, M. U., Khan, H. F., Masud, M., Kallu, K. D., & Zafar, A. (2020). A machine learning framework to identify the hotspot in photovoltaic module using infrared thermography. *Solar Energy*, *208*, 643–651. https://doi.org/10.1016/j.solener.2020.08.027

4. Amiri, A. F., Kichou, S., Oudira, H., Chouder, A., & Silvestre, S. (2024). Fault Detection and Diagnosis of a Photovoltaic System Based on Deep Learning Using the Combination of a Convolutional Neural Network (CNN) and Bidirectional Gated Recurrent Unit (Bi-GRU). *Sustainability (Switzerland)*, *16*(3), 1–21. https://doi.org/10.3390/su16031012

5. Baltacı, Ö., Kıral, Z., Dalkılınç, K., & Karaman, O. (2024). Thermal Image and Inverter Data Analysis for Fault Detection and Diagnosis of PV Systems. *Applied Sciences (Switzerland)*, *14*(9), 1–15. https://doi.org/10.3390/app14093671

6. Cipriani, G., D'Amico, A., Guarino, S., Manno, D., Traverso, M., & Di Dio, V. (2020). Convolutional neural network for dust and hotspot classification in PV modules. *Energies*, *13*(23), 1–17. https://doi.org/10.3390/en13236357

7. Dhimish, M., Theristis, M., & D'Alessandro, V. (2024). Photovoltaic hotspots: A mitigation technique and its thermal cycle. *Optik*, *300*, 1–12. https://doi.org/10.1016/j.ijleo.2024.171627

8. Goudelis, G., Lazaridis, P. I., &Dhimish, M. (2022). A Review of Models for Photovoltaic Crack and Hotspot Prediction. *Energies*, *15*(12), 1–24. https://doi.org/10.3390/en15124303

9. Huerta Herraiz, Á., Pliego Marugán, A., & García Márquez, F. P. (2020). Photovoltaic plant condition monitoring using thermal images analysis by convolutional neural network-based structure. *Renewable Energy*, *153*, 334–348. https://doi.org/10.1016/j.renene.2020.01.148

10. Karimi, M., Samet, H., Ghanbari, T., &Moshksar, E. (2020). A current based approach for hotspot detection in photovoltaic strings. *International Transactions on Electrical Energy Systems*, *30*(9), 1–18. https://doi.org/10.1002/2050-7038.12517

11. Kirubakaran, V., Preethi, D. M. D., Arunachalam, U., Rao, Y. K. S. S., Gatasheh, M. K., Hoda, N., &Anbese, E. M. (2022). Infrared Thermal Images of Solar PV Panels for Fault Identification Using Image Processing Technique. *International Journal of Photoenergy*, *2022*, 1–10. https://doi.org/10.1155/2022/6427076

12. Omaima Alshanqiti. (2026). Characterization of tri quasi purity applicable for (b1, b2)-regularities of an ordered semirings. *Results in Nonlinear Analysis*, *9*(2), 1–13.

13. Pathak, S. P., Patil, D. S., & Patel, S. (2022). Solar panel hotspot localization and fault classification using deep learning approach. *Procedia Computer Science*, *204*, 698–705. https://doi.org/10.1016/j.procs.2022.08.084

14. Pruthviraj, U., Kashyap, Y., Baxevanaki, E., &Kosmopoulos, P. (2023). Solar Photovoltaic Hotspot Inspection Using Unmanned Aerial Vehicle Thermal Images at a Solar Field in South India. *Remote Sensing*, *15*(7), 1–20. https://doi.org/10.3390/rs15071914

15. Sridharan, N. V., & Sugumaran, V. (2021). Convolutional Neural Network based Automatic Detection of Visible Faults in a Photovoltaic Module. *Energy Sources, Part A: Recovery, Utilization and Environmental Effects*, 1–16. https://doi.org/10.1080/15567036.2021.1905753

16. Su, B., Chen, H., Liu, K., & Liu, W. (2021). RCAG-Net: Residual Channelwise Attention Gate Network for Hot Spot Defect Detection of Photovoltaic Farms. *IEEE Transactions on Instrumentation and Measurement*, *70*, 1–14. https://doi.org/10.1109/TIM.2021.3054415

17. Su, B., Chen, H., & Zhou, Z. (2022). BAF-Detector: An Efficient CNN-Based Detector for Photovoltaic Cell Defect Detection. *IEEE Transactions on Industrial Electronics*, *69*(3), 3161–3171. https://doi.org/10.1109/TIE.2021.3070507

18. Ukiwe, E. K., Adeshina, S. A., Jacob, T., &Adetokun, B. B. (2024). Deep learning model for detection of hotspots using infrared thermographic images of electrical installations. *Journal of Electrical Systems and Information Technology*, *11*(1), 1–25. https://doi.org/10.1186/s43067-024-00148-y

19. Wang, F., Wang, Z., Chen, Z., Zhu, D., Gong, X., & Cong, W. (2023). An Edge-Guided Deep Learning Solar Panel Hotspot Thermal Image Segmentation Algorithm. *Applied Sciences (Switzerland)*, *13*(19), 1–16. https://doi.org/10.3390/app131911031

20. Winston, D. P., Murugan, M. S., Elavarasan, R. M., Pugazhendhi, R., Singh, O. J., Murugesan, P., Gurudhachanamoorthy, M., & Hossain, E. (2021). Solar PV's Micro Crack and Hotspots Detection Technique Using NN and SVM. *IEEE Access*, *9*, 127259–127269. https://doi.org/10.1109/ACCESS.2021.3111904

21. Wu, X., & Hao, X. (2023). SK-FRCNN: A Fault Detection Method for Hot Spots on Photovoltaic Panels. *IEEE Access*, *11*, 121379–121386. https://doi.org/10.1109/ACCESS.2023.3328332

22. Xiaoni, C., Wei, D., He, Y., & Shen, M. (2024). A fault diagnosis method of hot spots for photovoltaic clusters based on model parameters. *Energy Science and Engineering*, 3453–3464. https://doi.org/10.1002/ese3.1829